NeuroImage: Clinical 28 (2020) 102391

Contents lists available at ScienceDirect

NeuroImage: Clinical

journal homepage: www.elsevier.com/locate/ynicl

Increased iron-deposition in lateral-ventral substantia nigra pars compacta: A promising neuroimaging marker for Parkinson's disease

Naying He[a,1], Jason Langley[b,1], Daniel E. Huddleston[c], Shengdi Chen[d], Pei Huang[d], Huawei Ling[a], Fuhua Yan[a,*], Xiaoping Hu[b,e,*]

[a] Department of Radiology, Ruijin Hospital, Shanghai Jiao Tong University School of Medicine, Shanghai 200025, China
[b] Center for Advanced Neuroimaging, University of California, Riverside, CA, USA
[c] Department of Neurology, Emory University School of Medicine, Atlanta, GA, USA
[d] Department of Neurology and Institute of Neurology, Ruijin Hospital, Shanghai Jiao Tong University School of Medicine, Shanghai 200025, China
[e] Department of Bioengineering, University of California, Riverside, CA, USA

ARTICLE INFO

Keywords:
Parkinson's disease
R_2*
Substantia nigra pars compacta
Overlap percentage
Diagnostic biomarker

ABSTRACT

Background: To date there are no validated MRI biomarkers to assist diagnosis of Parkinson's disease (PD). Our aim was to investigate PD related iron changes in the substantia nigra pars compacta (SNpc) as defined by neuromelanin-sensitive MR contrast.

Methods: Thirty-nine PD participants and 33 healthy controls were scanned at 3.0-T using a 16-echo gradient echo sequence to create R_2* maps for the evaluation of iron content to find the overlap with a neuromelanin based SNpc mask. The SNpc overlap percentage with the R_2* map, and the R_2* values in both the whole SNpc and the overlap volume were compared between PD and control groups, and correlated with clinical features for PD participants. Finally, the diagnostic performance of the SNpc overlap percentage was evaluated using ROC analysis.

Results: PD related iron changes mostly occur in the lateral-ventral part of the neuromelanin SNpc. The R_2* values in the whole SNpc and the SNpc overlap volume, and the SNpc overlap percentage were larger in PD participants than in controls. Furthermore, the SNpc overlap percentage was positively correlated with the disease duration in PD. The SNpc overlap percentage provided excellent diagnostic accuracy for discriminating PD participants from controls (AUC = 0.93), while the R_2* values in the whole SNpc or the overlap volume were less effective.

Conclusion: The overlap between the iron content as determined by R_2* mapping and neuromelanin in the substantia nigra pars compacta has the potential to be a neuroimaging biomarker for diagnosing Parkinson's disease.

1. Introduction

Parkinson's disease (PD) is a movement disorder diagnosed clinically on the basis of supportive and exclusionary clinical findings. Supportive features include motor symptoms of rest tremor, bradykinesia, and rigidity, and recent consensus diagnostic criteria for PD also incorporate anosmia, a non-motor PD symptom (Postuma et al., 2015). DaTscan can be used to guide PD diagnosis (Postuma et al., 2015) but limited availability, cost, and use of radioisotopes hinders the widespread use of DaTscan.

Clinical diagnosis of PD is imperfect, and most clinicopathologic correlation studies find clinical diagnostic accuracy to be in the 70% to 90% range, with some variation attributable to the training of the diagnosing physician (Postuma et al., 2015; Rizzo et al., 2016). Inaccurate diagnosis may lead to increased patient morbidity due to incorrect treatments, and harms PD clinical research progress due to recruitment of patients who do not truly have PD. Thus, there is an urgent need for new PD imaging biomarkers to detect and quantify core aspects of PD neurodegeneration. Such biomarkers may be used to assist clinical diagnosis, and to assist participant selection and outcome measurement in clinical trials.

A primary characteristic of PD neurodegeneration is depigmentation

* Corresponding authors at: Department of Radiology, Ruijin Hospital, Shanghai Jiao Tong University School of Medicine, No.197 Ruijin Er Road, Shanghai 200025, China (F. Yan). Department of Bioengineering, University of California, Riverside, Materials Science and Engineering 205, USA (X. Hu).
E-mail addresses: yfh11655@rjh.com.cn (F. Yan), xhu@engr.ucr.edu (X. Hu).
[1] Both authors contributed equally to this work.

https://doi.org/10.1016/j.nicl.2020.102391
Received 4 March 2020; Received in revised form 9 July 2020; Accepted 17 August 2020
Available online 20 August 2020

of melanized neurons in substantia nigra pars compacta (SNpc), and the greatest loss of melanized neurons occurs in its lateral-ventral tier (Fearnley and Lees, 1991; Gibb and Lees, 1991). MRI pulse sequences sensitive to neuromelanin (NM) can be used to localize SNpc (Chen et al., 2014; Sasaki et al., 2006; Schwarz et al., 2011) and examination of SNpc of patients with PD using these sequences has revealed reductions in SNpc width (Reimao et al., 2015) or reductions in neuromelanin-sensitive contrast of patients with PD (Huddleston et al., 2017).

Iron deposition occurs in conjunction with the loss of melanized SNpc neurons (Morris and Edwardson, 1994) and several imaging studies have found increases in measures sensitive to iron in regions near SNpc (Du et al., 2018; Peran et al., 2010). Most studies (Aquino et al., 2014; Baudrexel et al., 2010; Du et al., 2011; Focke et al., 2011; Gorell et al., 1995; Graham et al., 2000; Isaias et al., 2016; Kosta et al., 2006; Martin et al., 2008; Mondino et al., 2002; Ordidge et al., 1994; Peran et al., 2010; Vymazal et al., 1999; Wallis et al., 2008) have attempted to localize the SNpc region of interest (ROI) in T_2-weighted images, which is difficult since T_2-weighted images are not sensitive to neuromelanin and lack definitive landmarks for SNpc (Langley et al., 2015). However, ROIs derived from neuromelanin-sensitive image data can be used to localize SNpc in T_2*-weighted images. Increased hypointensity in T_2*-weighted images has been observed in the lateral and ventral portions of the neuromelanin-sensitive SNpc ROI in PD patients (Langley et al., 2015, 2016, 2017).

R_2* relaxometry is sensitive to tissue iron deposition, and has been shown to be highly correlated with brain tissue iron content (Langkammer et al., 2010). Here, we will measure R_2* in the neuromelanin-sensitive MRI (NM-MRI) defined SNpc to quantitatively evaluate PD-related iron deposition. A previous study that found the percentage of overlap between T_2-weighted hypointensity and neuromelanin-sensitive contrast in the SNpc differentiates PD from controls with high accuracy (Langley et al., 2017). We hypothesize that iron content will be increased in the lateral-ventral SNpc, and we seek to evaluate the diagnostic utility of this measure.

2. Materials and methods

2.1. Participants

This prospective study was approved by the local ethics committee and data were collected between August 2014 and July 2015. All participants provided written informed consent. In this study, 39 right-handed PD participants (age: 63.4 ± 7.0 years; man/woman: 17/22) were recruited from local movement disorder outpatient clinic. All PD participants were diagnosed with PD according to the United Kingdom Parkinson's Disease Society Brain Bank criteria (Hughes et al., 1992). Demographic information including sex, age, and education was collected for each participant. Disease severity was evaluated using Hoehn & Yahr (H&Y) (Hoehn and Yahr, 1967) staging, and motor disability was assessed using the motor portion of the Unified Parkinson's Disease Rating Scale (UPDRS)-III (Fahn et al., 1987) in the ON medication state. Inclusion criteria for the PD group was a diagnosis of idiopathic PD and the exclusion criteria were: (1) Secondary parkinsonism which was caused by use of drugs (eg, antipsychotics, antiemetics, and drugs that deplete dopamine) and atypical parkinsonian symptoms (such as progressive supranuclear palsy, multiple system atrophy, dementia with Lewy bodies and corticobasal syndrome); (2) Mini-Mental State Exam (MMSE) score less than 24; (3) a history of cerebrovascular disease, seizures, brain surgery, brain tumor, moderate-to-severe head trauma or hydrocephalus; or (4) treatment with antipsychotic drugs or with any other drug possibly affecting clinical evaluation.

Thirty-three sex- and age-matched right-handed healthy controls (age: 63.8 ± 6.9 years; man/woman: 14/19) were recruited from the local community. Inclusion criteria for the control group were: (1) normal movement function and neurological status; (2) absence of neurological or psychiatric disease; (3) and a MMSE score equal to or greater than 24.

2.2. MRI scanning

All participants were imaged with a 3.0-T scanner (Signa HDxt; GE Healthcare) equipped with an eight-channel receive-only head coil. A 3D multi-echo gradient echo (GRE) sequence was used to acquire images suitable for measurement of R_2* with the following parameters: repetition time (TR) = 59.3 ms; number of echoes = 16; first echo time (TE_1) = 2.7 ms; echo spacing (ΔTE) = 2.9 ms; flip angle (FA) = 12°; field of view (FOV) = 22 × 22 cm^2; resolution = 0.86 × 0.86 × 1.0 mm^3; sensitivity encoding (SENSE) acceleration factor = 2; and total acquisition time = 10 min 42 s. Whole brain anatomical images were acquired with a T_1-weighted fast spoiled GRE sequence for common space registration. Imaging parameters for this sequence were: TR = 5.5 ms; TE = 1.7 ms; inversion time (TI) = 450 ms, resolution = 1 × 1 × 1 mm^3; and FA = 12°.

2.3. Standard space transformation

Imaging data were analyzed with FMRIB Software Library (FSL). A transformation was derived between individual subject space to Montreal Neurological Institute (MNI) 152T1-weighted space using FMRIB's Linear Image Registration Tool (FLIRT) and FMRIB's Nonlinear Image Registration Tool (FNIRT) in the FSL software package using the following steps: First, the brain extracted T_1-weighted image in individual space was aligned with the MNI brain extracted image using FLIRT. Second, using this T_1-weighted image, a transformation between individual space and common space was generated using FNIRT and the inverse of this transform was then used to map the NM mask from common space back to the original T_1 individual space. Finally, the first echo from the GRE image was registered to the T_1-weighted image.

2.4. R_2* calculation

R_2* was calculated from all echoes acquired in the multi-echo GRE sequence using a custom script in MATLAB by fitting a mono-exponential model to the GRE images.

$$S_i = S_0 \exp(-R_2^* TE) \quad [1]$$

where S_0 denotes a fitting constant and S_i denotes the signal of a voxel at the ith echo time.

2.5. SN segmentation

The processing pipeline for the SN segmentation and the creation of the overlap mask is shown in Fig. 1. The SN was segmented in R_2* maps using the following procedure: first, a tegmentum reference region, derived by drawing a 3 mm × 3 mm ROI in the cerebral peduncle in MNI152 space, was transformed from standard space to R_2* maps using the transforms described above and the mean (μ_{REF}) and standard deviation (σ_{REF}) in the reference ROI was recorded. Next, a standard space probabilistic T_2*-weighted SN ROI, derived from a previous study (Langley et al., 2019) and encompassing the SN in the R_2* image, was transformed from standard space to R_2* maps then thresholded at a level of 10%, binarized, and dilated. Voxels with R_2* values inside the dilated ROI exceeding a threshold of $\mu_{REF} + 3\ \sigma_{REF}$ were considered to be part of the SN. The entire area of elevated R_2* values was denoted by $SN_{R2*HIROI}$.

Since NM-MRI images were not acquired, a NM-MRI based SNpc template (Langley et al., 2015) was used to localize SNpc. The SNpc template was constructed from 11 younger healthy participants with no known neurological abnormalities (6 male, 5 female; mean age: 30.3 years ± 5.3 years). The SNpc template was transformed from standard space to native R_2* images, thresholded at a level of 0.6, and

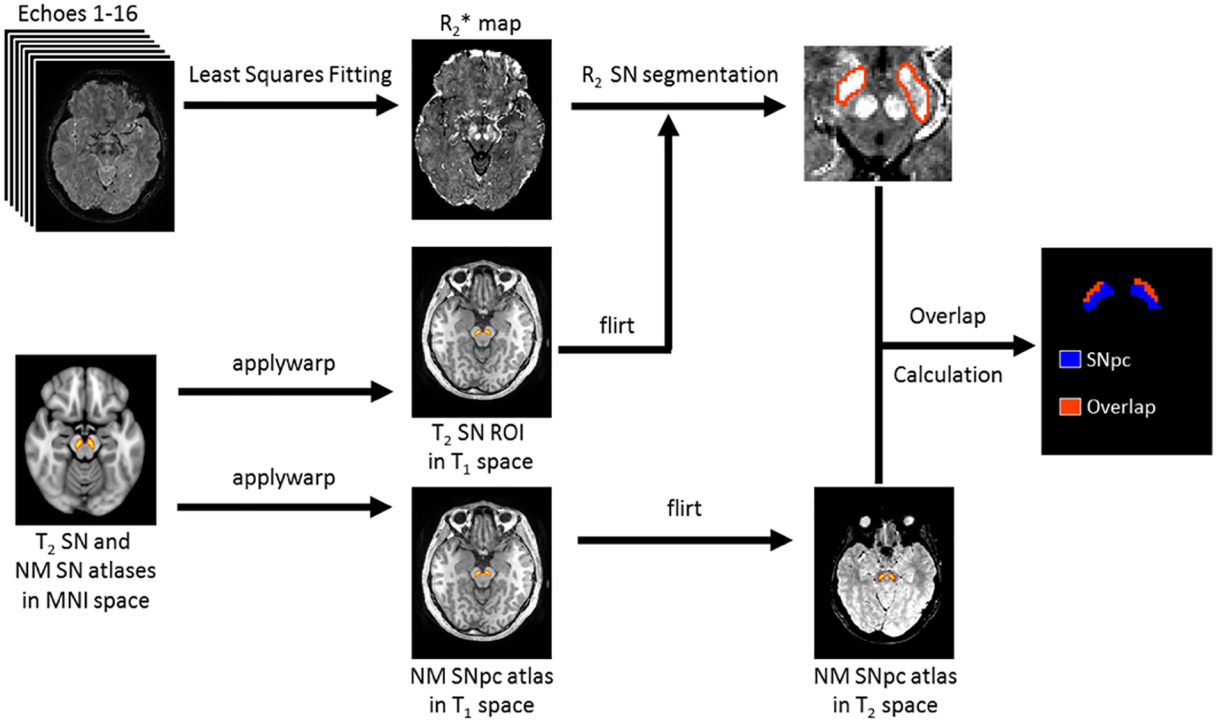

Fig. 1. The processing pipeline for the SN segmentation and the creation of the overlap mask.

Table 1
Demographic information and clinical characteristics of the HC and PD cohorts.

Variable (mean ± SD)	HC (n = 33)	PD (n = 39)	p value
Sex (man/woman)	14/19	17/22	0.921
Age (years)	63.8 ± 6.9	63.4 ± 7.0	0.416
Education (years)	10.5 ± 3.1	11.8 ± 3.5	0.581
Disease Duration (years)	/	6.1 ± 4.5	/
Hoehn and Yahr Scale	/	1.7 ± 0.078	/
UPDRS-III score	/	22.13 ± 12.64	/

UPDRS unified Parkinson's disease rating scale, PD Parkinson's disease, HC healthy control.

binarized. Finally, the SNpc overlap percentage between the whole SNpc and SN in R_2* images was calculated. The SNpc overlap percentage is defined as follows:

$$SNpcoverlappercentage = \frac{Volume(SN_{pc} \cap SN_{R2*HIROI})}{Volume(SN_{pc})} \quad (1)$$

where SN_{NM} and $SN_{R2*HIROI}$ denote the NM MRI based SNpc and the R_2* SN region, respectively. In order to display graphically the totality of all the overlap results, a color coded probability map was created representing the area of iron increases in the SNpc.

2.6. Statistical analysis

2.6.1. Demographic and clinical feature analysis

A chi-square test was used to evaluate the sex between groups. An independent two-sample t-test was performed to compare age and clinical features between groups. All of the statistical calculations were performed using SPSS (Version 20).

Image analysis:

SN, as seen in T_2- or T_2*-weighted images is spatially incongruent to the SN seen in NM-MRI images with small overlap between the T_2*- and NM-MRI SNs (Langley et al., 2015). The overlapping region is situated in the lateral and ventral portion of the NM-MRI SN. Prior imaging studies have found increased areas of T_2*-weighted hypointensity in the lateral and ventral portions of the NM-MRI SN of PD patients as compared to controls (Langley et al., 2017). Thus, we hypothesized that SNpc iron levels would be increased in the PD group. Group comparison of mean R_2* in the entire SNpc volume as well as in the SNpc overlap volume was made using a two tailed two-sample t-test. A correlation analysis was performed between each of following three parameters: the mean R_2* in the SNpc overlap volume, the mean R_2* in the SNpc template volume, and the SNpc overlap percentage with disease duration and UPDRS-III score in the PD group controlling for age. Diagnostic performance of the same three parameters was performed using a receiver operating characteristics (ROC) analysis. The threshold of statistical significance was set to $p < 0.05$.

3. Results

The demographic and clinical data for PD and control groups are shown in Table 1. No significant differences were observed in age (p = 0.42) or sex (p = 0.92) between the two groups.

The SNpc overlap percentage represents the occurrence of high R_2* values in the neuromelanin-defined SNpc. The occurrence of overlap is shown in Fig. 2 in which the range of red to yellow (the SNpc overlap region) represents the probability of finding increased iron from the R_2* maps in a given spatial location in the template space for the PD cohort and control cohort. It can be seen from the coronal image in Fig. 2 that this overlap region is located in the lateral-ventral part of the SNpc. Increased SNpc overlap percentage was observed in the PD cohort as compared to controls (PD: 0.33 ± 0.15, controls: 0.07 ± 0.07, $p = 4.70 \times 10^{-13}$, Fig. 3C). A significant increase in R_2* was seen for the patients with PD relative to controls in the whole NM SNpc template volume (PD: 34.8 ± 4.7/s, controls: 31.4 ± 4.2/s p = 0.0016, Fig. 3A) and a trend toward increased R_2* was observed in the SNpc overlap volume (PD: 35.9 ± 5.9/s, controls: 33.2 ± 5.7/s, p = 0.0572, Fig. 3B).

ROC analysis of R_2* in the SNpc overlap volume, the SNpc total volume and the SNpc overlap percentage in PD and controls yielded an area under the curve (AUC) of 0.65 (95% CI: 0.52–0.78; p = 0.030), 0.71 (95% CI: 0.59–0.83; p = 0.003) and 0.93 (95% CI: 0.87–0.99;

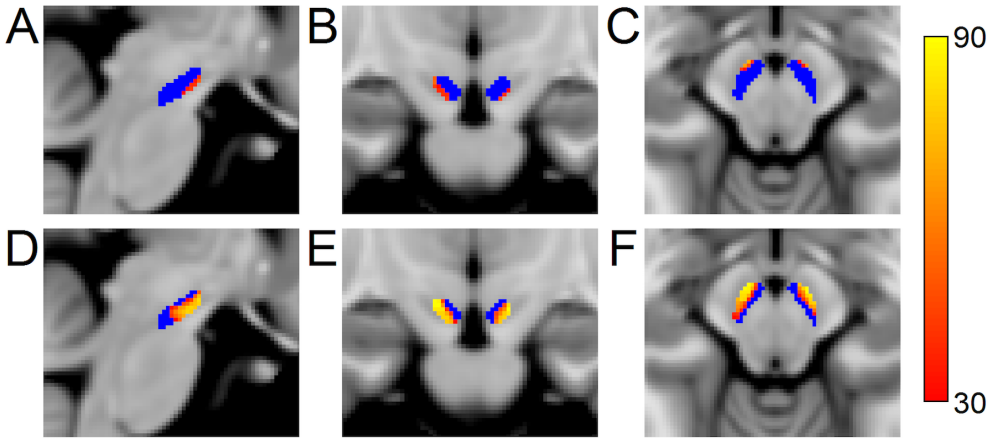

Fig. 2. The overlap population atlases for the HC (top row) and PD (bottom row) cohort. Sagittal, coronal, and axial views of the overlap population atlases are shown in the left column (A and D), middle column (B and E), and right column (C and F), respectively. The neuromelanin-sensitive SNpc is shown in blue plus red-yellow and regions of SNpc undergoing iron deposition are shown in red-yellow. Higher values indicate that more individuals share iron deposition. The color bar on the right side denotes the overlap probability between the SNpc and the R_2* hyperintense substantia nigra as determined from both cohorts separately. (For interpretation of the references to color in this figure legend, the reader is referred to the web version of this article.)

$p = 3.96 \times 10^{-10}$), respectively (Fig. 4). The ability to distinguish PD from HC was clearly better using the SNpc overlap percentage than using R_2* value in either the whole SNpc or the SNpc overlap volume as the discriminating factor.

The SNpc overlap percentage was positively correlated with disease duration ($R = 0.438$; $p = 0.006$) (Fig. 5A) in the PD cohort. The overlap changes range from nearly 0% for the very early stage patients up to roughly 60% for the long disease duration patients. There was no significant correlation for the SNpc overlap percentage with UPDRS-III ($R = 0.124$; $p = 0.459$) (Fig. 5D). Also, no significant relationships were observed between R_2* in the whole SNpc volume (UPDRS-III: $R = -0.133$; $p = 0.426$; disease duration: $R = 0.290$; $p = 0.078$) (Fig. 5B, 5E) or in the overlap volume (UPDRS-III: $R = -0.170$; $p = 0.307$; disease duration: $R = 0.236$; $p = 0.154$) (Fig. 5C, 5F) with either UPDRS-III or disease duration in PD.

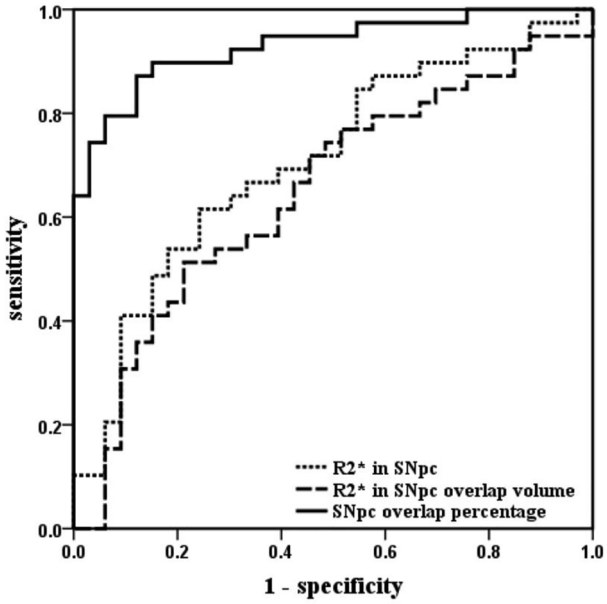

Fig. 4. Graph shows receiver operating characteristic curves to assess utility of three metrics (R_2* in SNpc, R_2* in SNpc overlap volume, and SNpc overlap percentage) for discriminating patients with PD and healthy controls.

4. Discussion

In this study, a SNpc atlas derived from neuromelanin-sensitive images was employed to evaluate SNpc iron deposition. We found that the percentage of SNpc exhibiting increased R_2* (SNpc overlap percentage) provided excellent diagnostic accuracy (AUC = 0.93) for discriminating patients with PD from healthy controls. This region was located in the lateral-ventral part of the NM-MRI defined SNpc, which is in agreement with previous histological evidence and a previous MRI study that used T_2*-weighted imaging to assess SNpc overlap percentage (Fearnley and Lees, 1991; Langley et al., 2017). Further, the SNpc overlap percentage was positively correlated with the PD disease duration in this study.

We found the overlap of iron sensitive and neuromelanin sensitive SN masks to be approximately 9% in the control cohort presented in this work. The nonzero overlap of the T_2*-weighted (or iron sensitive) SN mask and neuromelanin sensitive SNpc mask agrees with prior histological studies which showed that clusters of dopaminergic neurons from the SNpc penetrate into the SNr (Haber, 2003). We previously reported a mean overlap of T_2*-weighted hypointense SN and neuromelanin SN masks of ~12% in a cohort of young, healthy controls (Langley et al., 2015). The present result accords well with our prior work despite the age difference between the two control cohorts, and this agreement may suggest that iron deposition in the SNpc derived

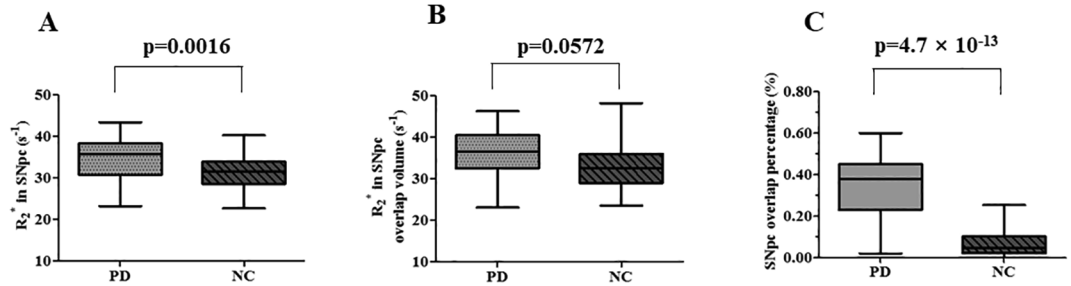

Fig. 3. Group analysis of R_2* values in both the entire SNpc volume (A) and the SNpc overlap volume (B) for PD and HC cohorts. A comparison of SNpc overlap percentage in PD and HC is shown in C. This figure shows the maximum (upper line), minimum (lower line), median (center line) and quartile (box) of the data.

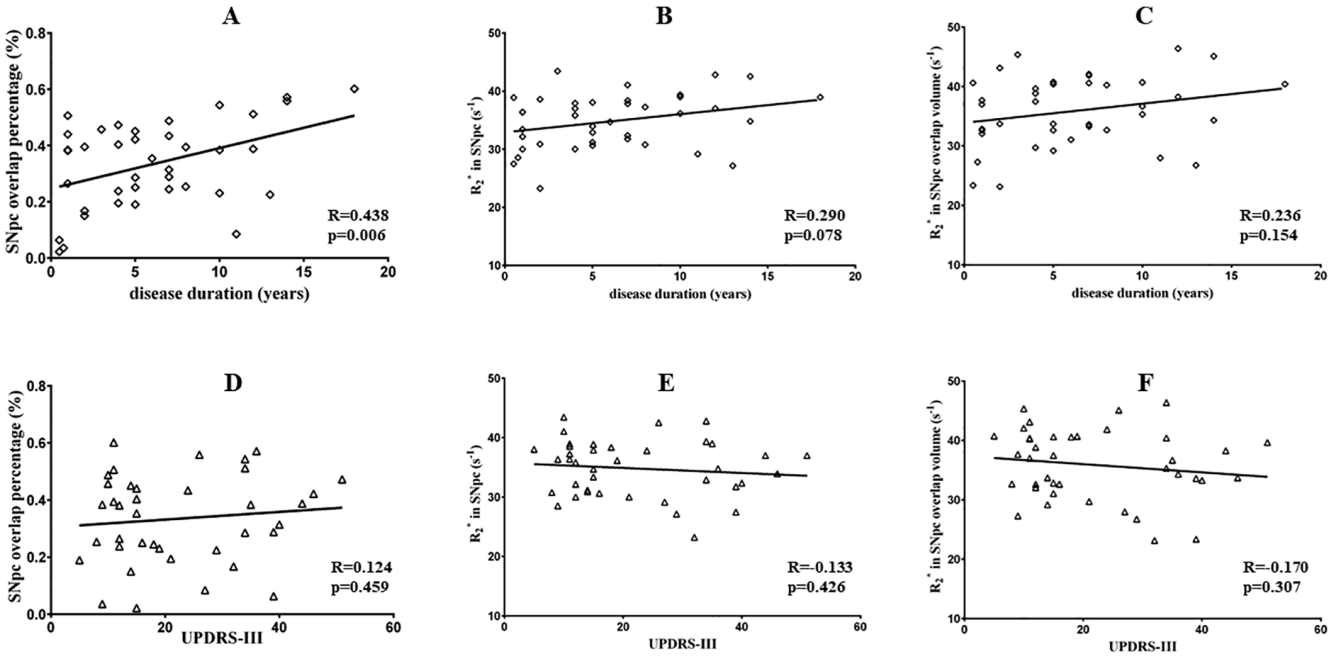

Fig. 5. The SNpc overlap percentage (A) was positively correlated with disease duration in patients with PD. There was no significant correlation for the SNpc overlap percentage with UPDRS-III B). No significant relationships were observed between R_2* in the whole SNpc volume (B, E) or in the overlap volume (C, F) with either UPDRS-III or disease duration in PD.

from NM-MRI is not dependent on age in normal subjects and is primarily due to PD. Additionally, SNpc R_2* values in the control group are in line with those published in an earlier study examining age-related iron deposition in SNpc (Langley et al., 2020).

In early stage PD, histological studies have shown that the dopaminergic neuronal loss is most pronounced in the caudal lateral-ventral tier of SNpc while the dorsal tier is relatively preserved (Fearnley and Lees, 1991; Jellinger, 2012). Our findings also show an increase in iron deposition in the lateral and ventral portions of the SNpc. This increase in iron may be due to the accumulation of iron from the depigmented neuromelanin granules (Jellinger et al., 1992). Several histopathological, biochemical and in-vivo brain imaging studies have shown an increase in total iron concentration in the SN of patients with PD (Dexter et al., 1991; Zecca et al., 2004), with higher iron content corresponding to more severe disease (PD) (Youdim et al., 1990). In addition, prior imaging studies have found an increase in SN, as defined in T_2-weighted images, iron content for patients with PD as compared to controls (Du et al., 2018, 2011; He et al., 2015; Martin et al., 2008; Peran et al., 2010). In accordance with these earlier results, we observed an increase in mean R_2* values in the entire SNpc of patients with PD, indicating increased iron deposition. However, no significant correlations were observed between mean SNpc R_2* values and clinical measures.

Since SNpc degeneration in early stages of PD is localized to the lateral-ventral tier (Fearnley and Lees, 1991; Jellinger, 2012), examination of this region may provide more accurate information regarding the pathologic severity of PD. There was an apparent increase in mean R_2* in the overlap region, but it was not as sensitive to PD-related changes as mean R_2* in the entire SNpc. The sensitivity of the SNpc overlap region to PD-related iron deposition may be dampened by the small overlap region in controls. As the SNpc overlap region is smaller than the entire SNpc, R_2* increases in the SNpc overlap region in controls will have a more pronounced contribution to mean R_2* than when R_2* is measured in the entire SNpc, effectively raising mean overlap R_2* and reducing the effect size.

Neuronal loss in SNpc is not uniform with most of the loss occurring in densely packed clusters of neurons named nigrosomes (Damier et al., 1999). The largest nigrosome, nigrosome-1, experiences the greatest loss of melanized neurons (Damier et al., 1999). Nigrosome-1 can be seen as a hyperintense region embedded in the hypointense SN in T_2- or T_2*-weighted images of control subjects (Blazejewska et al., 2013). PD-related iron deposition, associated with neuronal loss, causes a reduction in T_2- or T_2*-weighted signal in nigrosome-1 and the marker is not present in PD subjects (Blazejewska et al., 2013; Cheng et al., 2020; Schwarz et al., 2018). Intriguingly, nigrosome-1 is located in the lateral and ventral regions of the neuromelanin-defined SNpc (Huddleston et al., 2018) and iron deposition in the lateral-ventral tier of SNpc observed in this work may be imaging similar aspects of PD-pathology.

Interestingly, a significant correlation was observed between SNpc overlap percentage and disease duration. This result is in agreement with an earlier histology study examining total iron concentration and disease severity (Youdim et al., 1990). Since this study uses a cross-sectional cohort, a longitudinal study measuring SNpc overlap percentage in PD participants at different time points is necessary to verify this correlation. A longitudinal study of individuals with PD using this approach examining SNpc overlap percentage will allow for assessment of within-participant progression and may identify biomarkers sensitive to treatment response in neuroprotective therapeutic trials or for monitoring disease progression.

Although there is a correlation between the SNpc overlap percentage and disease duration, there was no correlation between the mean R_2* values in both SNpc overlap volume and entire SNpc and disease duration or ON UPDRS-III score. In this study, UPDRS-III was measured in the ON medication state and may not accurately represent motor dysfunction and reduce the concurrence with SNpc iron content.

The ROC analysis found SNpc overlap percentage (AUC = 0.93) to be the best diagnostic measure for discriminating patients with PD from healthy controls among the iron-sensitive measures included in this study. The AUC of SNpc overlap percentage compares well to AUCs from prior studies examining SN iron deposition (Cheng et al., 2020; Li et al., 2019) or NM-MRI measures (Ariz et al., 2019; Huddleston et al., 2017; Schwarz et al., 2016; Shinde et al., 2019), which have AUCs between 0.7 and 0.9. As each imaging marker is sensitive to a single aspect of PD pathology, it is likely that a single imaging marker will not fully capture all facets of PD pathology. A combination of imaging markers incorporating many different aspects of PD pathology in SNpc

(such as depigmentation of melanized neurons and associated iron deposition in the lateral-ventral tier, SNpc volume, and SNpc iron deposition) may improve diagnostic performance and lead to a clinically useful marker for diagnosis of PD.

While nigral iron deposition has long been reported as a feature of PD neurodegeneration, the image processing approach applied here captures PD associated iron deposition *in vivo* both reproducibly and with a very strong group effect. This work also replicates a similar study of nigral iron/neuromelanin MR contrast overlap percentage in PD and controls (Langley et al., 2017). Further, as seen in the supplementary materials document, we found that the overlap percentage and spatial pattern of overlap is consistent in two SNpc atlases. Given these characteristics, iron/neuromelanin overlap percentage appears to be a promising candidate imaging marker for differentiating PD from HC, and is worthy of further development for translational applications, particularly those differentiating PD from atypical parkinsonian syndromes.

This study is not without caveats. First, PD phenotypes are hypothesized to effect structures and functional circuits differently. For example, patients with tremor dominant PD will have less SNpc depigmentation and elevated dentate nucleus iron than other PD phenotypes (He et al., 2017, 2015). In this study, the different phenotypes of PD have not been taken into account to improve power. Second, there were only a limited number of advanced stage patients with PD. Also, a longitudinal study with a much larger cohort of patients with PD and HC is needed to validate this approach and prove the disease progression. Finally, NM-MRI data was not collected in this study and we cannot remark on the relationship between iron deposition and NM loss. Reduced neuromelanin-sensitive contrast has been observed in the lateral-ventral tier of SNpc (Huddleston et al., 2017) and a multimodal study examining iron deposition and neuromelanin depletion may elucidate the role of iron deposition and SNpc depigmentation.

In conclusion, the overlap between the iron content as determined by R_2* mapping and NM in SNpc has the potential to be a neuroimaging biomarker for PD.

CRediT authorship contribution statement

Naying He: Writing - original draft, Writing - review & editing, Investigation, Data curation, Formal analysis. **Jason Langley:** Writing - original draft, Writing - review & editing, Conceptualization, Formal analysis. **Daniel E. Huddleston:** Writing - review & editing. **Shengdi Chen:** Data curation, Formal analysis, Writing - review & editing. **Pei Huang:** Data curation, Formal analysis, Writing - review & editing. **Huawei Ling:** Writing - review & editing. **Fuhua Yan:** Supervision, Funding acquisition, Resources, Writing - review & editing. **Xiaoping Hu:** Conceptualization, Supervision, Writing - review & editing.

Declaration of Competing Interest

The authors declare that they have no known competing financial interests or personal relationships that could have appeared to influence the work reported in this paper.

Acknowledgements

This work was supported by the Shanghai Sailing Program (18YF1414700); National Natural Science Fund (81801652, 81971576); the Science and Technology Commission of Shanghai Municipality (17411952700); the Innovative Research Team of High-level Local Universities in Shanghai; the Michael J. Fox Foundation (MJF 10854); The American Parkinson's Disease Association Emory Center for Advanced Research; The Lewy Body Dementia Association Emory Research Center of Excellence ;and the NIH grant funding (NIH-NINDS 1K23NS105944-03; NIH-NIA 1R34AG056639-02).

Appendix A. Supplementary data

Supplementary data to this article can be found online at https://doi.org/10.1016/j.nicl.2020.102391.

References

Aquino, D., Contarino, V., Albanese, A., Minati, L., Farina, L., Grisoli, M., Elia, A., Bruzzone, M.G., Chiapparini, L., 2014. Substantia nigra in Parkinson's disease: a multimodal MRI comparison between early and advanced stages of the disease. Neurol. Sci. 35, 753–758.

Ariz, M., Abad, R.C., Castellanos, G., Martinez, M., Munoz-Barrutia, A., Fernandez-Seara, M.A., Pastor, P., Pastor, M.A., Ortiz-de-Solorzano, C., 2019. Dynamic atlas-based segmentation and quantification of Neuromelanin-Rich brainstem structures in Parkinson Disease. IEEE Trans. Med. Imaging 38, 813–823.

Baudrexel, S., Nurnberger, L., Rub, U., Seifried, C., Klein, J.C., Deller, T., Steinmetz, H., Deichmann, R., Hilker, R., 2010. Quantitative mapping of T1 and T2* discloses nigral and brainstem pathology in early Parkinson's disease. NeuroImage 51, 512–520.

Blazejewska, A.I., Schwarz, S.T., Pitiot, A., Stephenson, M.C., Lowe, J., Bajaj, N., Bowtell, R.W., Auer, D.P., Gowland, P.A., 2013. Visualization of nigrosome 1 and its loss in PD: pathoanatomical correlation and in vivo 7 T MRI. Neurology 81, 534–540.

Chen, X., Huddleston, D.E., Langley, J., Ahn, S., Barnum, C.J., Factor, S.A., Levey, A.I., Hu, X., 2014. Simultaneous imaging of locus coeruleus and substantia nigra with a quantitative neuromelanin MRI approach. Magn. Reson. Imaging 32, 1301–1306.

Cheng, Z., He, N., Huang, P., Li, Y., Tang, R., Sethi, S.K., Ghassaban, K., Yerramsetty, K.K., Palutla, V.K., Chen, S., Yan, F., Haacke, E.M., 2020. Imaging the Nigrosome 1 in the substantia nigra using susceptibility weighted imaging and quantitative susceptibility mapping: an application to Parkinson's disease. Neuroimage Clin. 25, 102103.

Damier, P., Hirsch, E.C., Agid, Y., Graybiel, A.M., 1999. The substantia nigra of the human brain. II. Patterns of loss of dopamine-containing neurons in Parkinson's disease. Brain 122 (Pt 8), 1437–1448.

Dexter, D.T., Carayon, A., Javoy-Agid, F., Agid, Y., Wells, F.R., Daniel, S.E., Lees, A.J., Jenner, P., Marsden, C.D., 1991. Alterations in the levels of iron, ferritin and other trace metals in Parkinson's disease and other neurodegenerative diseases affecting the basal ganglia. Brain 114 (Pt 4), 1953–1975.

Du, G., Lewis, M.M., Sica, C., He, L., Connor, J.R., Kong, L., Mailman, R.B., Huang, X., 2018. Distinct progression pattern of susceptibility MRI in the substantia nigra of Parkinson's patients. Mov. Disord. 33, 1423–1431.

Du, G., Lewis, M.M., Styner, M., Shaffer, M.L., Sen, S., Yang, Q.X., Huang, X., 2011. Combined R2* and diffusion tensor imaging changes in the substantia nigra in Parkinson's disease. Mov. Disord. 26, 1627–1632.

Fahn, S., Elton, R.L., Committee, U.D., 1987. Unified Parkinson's disease rating scale. Recent Dev. Parkinson's Dis. 2, 153–163.

Fearnley, J.M., Lees, A.J., 1991. Ageing and Parkinson's disease: substantia nigra regional selectivity. Brain 114 (Pt 5), 2283–2301.

Focke, N.K., Helms, G., Pantel, P.M., Scheewe, S., Knauth, M., Bachmann, C.G., Ebentheuer, J., Dechent, P., Paulus, W., Trenkwalder, C., 2011. Differentiation of typical and atypical Parkinson syndromes by quantitative MR imaging. AJNR Am. J. Neuroradiol. 32, 2087–2092.

Gibb, W.R., Lees, A.J., 1991. Anatomy, pigmentation, ventral and dorsal subpopulations of the substantia nigra, and differential cell death in Parkinson's disease. J. Neurol. Neurosurg. Psychiatry 54, 388–396.

Gorell, J.M., Ordidge, R.J., Brown, G.G., Deniau, J.C., Buderer, N.M., Helpern, J.A., 1995. Increased iron-related MRI contrast in the substantia nigra in Parkinson's disease. Neurology 45, 1138–1143.

Graham, J.M., Paley, M.N., Grunewald, R.A., Hoggard, N., Griffiths, P.D., 2000. Brain iron deposition in Parkinson's disease imaged using the PRIME magnetic resonance sequence. Brain 123 (Pt 12), 2423–2431.

Haber, S.N., 2003. The primate basal ganglia: parallel and integrative networks. J. Chem. Neuroanat. 26, 317–330.

He, N., Huang, P., Ling, H., Langley, J., Liu, C., Ding, B., Huang, J., Xu, H., Zhang, Y., Zhang, Z., Hu, X., Chen, S., Yan, F., 2017. Dentate nucleus iron deposition is a potential biomarker for tremor-dominant Parkinson's disease. NMR Biomed. 30.

He, N., Ling, H., Ding, B., Huang, J., Zhang, Y., Zhang, Z., Liu, C., Chen, K., Yan, F., 2015. Region-specific disturbed iron distribution in early idiopathic Parkinson's disease measured by quantitative susceptibility mapping. Hum. Brain Mapp. 36, 4407–4420.

Hoehn, M.M., Yahr, M.D., 1967. Parkinsonism: onset, progression and mortality. Neurology 17, 427–442.

Huddleston, D.E., Langley, J., Dusek, P., He, N., Faraco, C.C., Crosson, B., Factor, S., Hu, X.P., 2018. Imaging parkinsonian pathology in substantia nigra with MRI. Curr. Radiol. Rep. 6, 15.

Huddleston, D.E., Langley, J., Sedlacik, J., Boelmans, K., Factor, S.A., Hu, X.P., 2017. In vivo detection of lateral-ventral tier nigral degeneration in Parkinson's disease. Hum. Brain Mapp. 38, 2627–2634.

Hughes, A.J., Daniel, S.E., Kilford, L., Lees, A.J., 1992. Accuracy of clinical diagnosis of idiopathic Parkinson's disease: a clinico-pathological study of 100 cases. J. Neurol. Neurosurg. Psychiatry 55, 181–184.

Isaias, I.U., Trujillo, P., Summers, P., Marotta, G., Mainardi, L., Pezzoli, G., Zecca, L., Costa, A., 2016. Neuromelanin imaging and dopaminergic loss in Parkinson's disease. Front. Aging Neurosci. 8, 196.

Jellinger, K., Kienzl, E., Rumpelmair, G., Riederer, P., Stachelberger, H., Ben-Shachar, D., Youdim, M.B., 1992. Iron-melanin complex in substantia nigra of parkinsonian brains: an x-ray microanalysis. J. Neurochem. 59, 1168–1171.

Jellinger, K.A., 2012. Neuropathology of sporadic Parkinson's disease: evaluation and

changes of concepts. Mov. Disord. 27, 8–30.
Kosta, P., Argyropoulou, M.I., Markoula, S., Konitsiotis, S., 2006. MRI evaluation of the basal ganglia size and iron content in patients with Parkinson's disease. J. Neurol. 253, 26–32.
Langkammer, C., Krebs, N., Goessler, W., Scheurer, E., Ebner, F., Yen, K., Fazekas, F., Ropele, S., 2010. Quantitative MR imaging of brain iron: a postmortem validation study. Radiology 257, 455–462.
Langley, J., He, N., Huddleston, D.E., Chen, S., Yan, F., Crosson, B., Factor, S., Hu, X., 2019. Reproducible detection of nigral iron deposition in 2 Parkinson's disease cohorts. Mov. Disord. 34, 416–419.
Langley, J., Huddleston, D.E., Chen, X., Sedlacik, J., Zachariah, N., Hu, X., 2015. A multicontrast approach for comprehensive imaging of substantia nigra. NeuroImage 112, 7–13.
Langley, J., Huddleston, D.E., Merritt, M., Chen, X., McMurray, R., Silver, M., Factor, S.A., Hu, X., 2016. Diffusion tensor imaging of the substantia nigra in Parkinson's disease revisited. Hum. Brain Mapp. 37, 2547–2556.
Langley, J., Huddleston, D.E., Sedlacik, J., Boelmans, K., Hu, X.P., 2017. Parkinson's disease-related increase of T2*-weighted hypointensity in substantia nigra pars compacta. Mov. Disord. 32, 441–449.
Langley, J., Hussain, S., Flores, J.J., Bennett, I.J., Hu, X., 2020. Characterization of age-related microstructural changes in locus coeruleus and substantia nigra pars compacta. Neurobiol. Aging 87, 89–97.
Li, G., Zhai, G., Zhao, X., An, H., Spincemaille, P., Gillen, K.M., Ku, Y., Wang, Y., Huang, D., Li, J., 2019. 3D texture analyses within the substantia nigra of Parkinson's disease patients on quantitative susceptibility maps and R2(*) maps. NeuroImage 188, 465–472.
Martin, W.R., Wieler, M., Gee, M., 2008. Midbrain iron content in early Parkinson disease: a potential biomarker of disease status. Neurology 70, 1411–1417.
Mondino, F., Filippi, P., Magliola, U., Duca, S., 2002. Magnetic resonance relaxometry in Parkinson's disease. Neurol. Sci. 23 (Suppl. 2), S87–88.
Morris, C.M., Edwardson, J.A., 1994. Iron histochemistry of the substantia nigra in Parkinson's disease. Neurodegeneration 3, 277–282.
Ordidge, R.J., Gorell, J.M., Deniau, J.C., Knight, R.A., Helpern, J.A., 1994. Assessment of relative brain iron concentrations using T2-weighted and T2*-weighted MRI at 3 Tesla. Magn. Reson. Med. 32, 335–341.
Peran, P., Cherubini, A., Assogna, F., Piras, F., Quattrocchi, C., Peppe, A., Celsis, P., Rascol, O., Demonet, J.F., Stefani, A., Pierantozzi, M., Pontieri, F.E., Caltagirone, C., Spalletta, G., Sabatini, U., 2010. Magnetic resonance imaging markers of Parkinson's disease nigrostriatal signature. Brain 133, 3423–3433.
Postuma, R.B., Berg, D., Stern, M., Poewe, W., Olanow, C.W., Oertel, W., Obeso, J., Marek, K., Litvan, I., Lang, A.E., Halliday, G., Goetz, C.G., Gasser, T., Dubois, B., Chan, P., Bloem, B.R., Adler, C.H., Deuschl, G., 2015. MDS clinical diagnostic criteria for Parkinson's disease. Mov. Disord. 30, 1591–1601.
Reimao, S., Pita Lobo, P., Neutel, D., Correia Guedes, L., Coelho, M., Rosa, M.M., Ferreira, J., Abreu, D., Goncalves, N., Morgado, C., Nunes, R.G., Campos, J., Ferreira, J.J., 2015. Substantia nigra neuromelanin magnetic resonance imaging in de novo Parkinson's disease patients. Eur. J. Neurol. 22, 540–546.
Rizzo, G., Copetti, M., Arcuti, S., Martino, D., Fontana, A., Logroscino, G., 2016. Accuracy of clinical diagnosis of Parkinson disease: A systematic review and meta-analysis. Neurology 86, 566–576.
Sasaki, M., Shibata, E., Tohyama, K., Takahashi, J., Otsuka, K., Tsuchiya, K., Takahashi, S., Ehara, S., Terayama, Y., Sakai, A., 2006. Neuromelanin magnetic resonance imaging of locus ceruleus and substantia nigra in Parkinson's disease. NeuroReport 17, 1215–1218.
Schwarz, S.T., Mougin, O., Xing, Y., Blazejewska, A., Bajaj, N., Auer, D.P., Gowland, P., 2018. Parkinson's disease related signal change in the nigrosomes 1–5 and the substantia nigra using T2* weighted 7T MRI. Neuroimage Clin. 19, 683–689.
Schwarz, S.T., Rittman, T., Gontu, V., Morgan, P.S., Bajaj, N., Auer, D.P., 2011. T1-weighted MRI shows stage-dependent substantia nigra signal loss in Parkinson's disease. Mov. Disord. 26, 1633–1638.
Schwarz, S.T., Xing, Y., Tomar, P., Bajaj, N., Auer, D.P., 2016. In vivo assessment of brainstem depigmentation in Parkinson disease: potential as a severity marker for multicenter studies. Radiology 160662.
Shinde, S., Prasad, S., Saboo, Y., Kaushick, R., Saini, J., Pal, P.K., Ingalhalikar, M., 2019. Predictive markers for Parkinson's disease using deep neural nets on neuromelanin sensitive MRI. Neuroimage Clin. 22, 101748.
Vymazal, J., Righini, A., Brooks, R.A., Canesi, M., Mariani, C., Leonardi, M., Pezzoli, G., 1999. T1 and T2 in the brain of healthy subjects, patients with Parkinson disease, and patients with multiple system atrophy: relation to iron content. Radiology 211, 489–495.
Wallis, L.I., Paley, M.N., Graham, J.M., Grunewald, R.A., Wignall, E.L., Joy, H.M., Griffiths, P.D., 2008. MRI assessment of basal ganglia iron deposition in Parkinson's disease. J. Magn. Reson. Imaging 28, 1061–1067.
Youdim, M.B., Ben-Shachar, D., Yehuda, S., Riederer, P., 1990. The role of iron in the basal ganglion. Adv. Neurol. 53, 155–162.
Zecca, L., Youdim, M.B., Riederer, P., Connor, J.R., Crichton, R.R., 2004. Iron, brain ageing and neurodegenerative disorders. Nat. Rev. Neurosci. 5, 863–873.